PHILOSOPHICAL TRANSACTIONS OF THE ROYAL SOCIETY A MATHEMATICAL, PHYSICAL & ENGINEERING SCIENCES

Multistability, Oscillations and Travelling Waves in a Product-Feedback Autocatalator Model. I. The Well-Stirred System

S. M. Collier, J. H. Merkin and S. K. Scott

Phil. Trans. R. Soc. Lond. A 1992 **340**, 447-472
doi: 10.1098/rsta.1992.0076

Multistability, oscillations and travelling waves in a product-feedback autocatalator model. I. The well-stirred system

By S. M. Collier[1], J. H. Merkin[1] and S. K. Scott[2]

[1] *Department of Applied Mathematical Studies and* [2] *School of Chemistry, University of Leeds, Leeds LS2 9JT, U.K.*

Contents

The behaviour of a modified autocatalator model:

$$\begin{aligned} \mathrm{P}+\mathrm{C} &\rightarrow \mathrm{A}+\mathrm{C}, & \text{rate} &= k_0 pc, \\ \mathrm{A}+2\mathrm{B} &\rightarrow 3\mathrm{B}, & \text{rate} &= k_1 ab^2, \\ \mathrm{B} &\rightarrow \mathrm{C}, & \text{rate} &= k_2 b, \\ \mathrm{C} &\rightarrow \mathrm{D}, & \text{rate} &= k_3 c, \end{aligned}$$

is studied in a batch system with the 'pool chemical approximation' applied to the precursor P (i.e. we assume $p = p_0 =$ constant for all time). Only for the special case $k_0 p_0 = k_3$, for which there is a reduction to a two variable system, are 'classical' nonlinear dynamical responses exhibited, with multiple stationary states, Hopf bifurcation to stable or unstable limit cycles and extinction of oscillations via homoclinic orbit formation. Under limiting parameter values, the locus of homoclinic bifurcations can be obtained analytically. For the general cases of $k_0 p_0 < k_3$ and $k_3 p_0 > k_3$ the system is contracting or expanding respectively. For the contracting case, there may be an initial period of sustained but strictly transient bistability or

Phil. Trans R. Soc. Lond. A (1992) **340**, 447–472
Printed in Great Britain

oscillation, and a clear three-time period emerges, before the reaction dies out completely, with b and c tending to zero. For the expanding case, the reaction either dies out as above or follows a continuous growth in intermediate species concentrations and overall reaction rate. The behaviour in these general cases can be readily understood in great detail from a consideration of the stationary state and dynamic bifurcation structure for the reduced case.

1. Introduction

There is much interest in chemical wave propagation in systems that exhibit sustained oscillations under well-stirred conditions. The two variable autocatalator has been used successfully to model oscillatory behaviour in isothermal closed systems (Merkin *et al.* 1986, 1987*a*, *b*; Gray & Scott 1986). The basic scheme, as originally considered, assumes that some precursor P, which is in plentiful supply reacts slowly to produce an intermediate A. This species is converted to a second intermediate B via an overall process that is autocatalytic in B. Finally, the autocatalyst B undergoes a decay reaction, producing a final, stable product C. This scheme has subsequently been elaborated to include a direct, uncatalysed conversion of A to B, various additional autocatalytic channels and the direct conversion of A to C (Gray *et al.* 1988, 1989). The chemical viability and motivation for this prototype reaction scheme has been discussed fully in the recent review article by Gray (1988).

Merkin & Needham (1989) analysed the behaviour associated with this model but in that case the additional complication of the direct conversion of A to B ahead of the wave leads to an accelerating front. More recently, the basic scheme has been extended to include the effects of a second feedback. Scott & Tomlin (1990) introduced the idea of a thermal feedback mechanism based on a temperature-sensitive initiation process and an exothermic 'termination' step $\mathrm{B}\rightarrow\mathrm{C}$. This introduces a sequence of secondary bifurcations from the original oscillatory response, leading to complex behaviour and to chemical chaos. An alternative, chemical feedback arrangement retaining the isothermal character of the original scheme has also been studied (Peng *et al.* 1990; Scott *et al.* 1991). There, the previously inert product C now plays a chemical role, with an additional channel from the original reactant P to species A being catalysed by C, and there is also a decay from C to the new, final product D. Again, this extended scheme supports period-doubling cascades to chaotic solutions.

Here, we consider this modified version of the C-feedback autocatalator of Peng *et al.* We assume that the step from precursor P to intermediate A proceeds only through the catalysed channel. Thus, the scheme considered is

$$\mathrm{P}+\mathrm{C}\rightarrow\mathrm{A}+\mathrm{C}, \quad \text{rate} = k_0 pc, \tag{1a}$$

$$\mathrm{A}+2\mathrm{B}\rightarrow 3\mathrm{B}, \quad \text{rate} = k_1 ab^2, \tag{1b}$$

$$\mathrm{B}\rightarrow\mathrm{C}, \quad \text{rate} = k_2 b, \tag{1c}$$

$$\mathrm{C}\rightarrow\mathrm{D}, \quad \text{rate} = k_3 c, \tag{1d}$$

If the concentrations of the intermediate species B and C ahead of the wave are initially zero, the system there is 'frozen', with zero reaction rate, until seeded by the diffusion of intermediates from the front. This is a consequence of neglecting the uncatalysed reactions: the inclusion of these steps provides a 'cold boundary

problem' similar to that encountered in non-isothermal flame studies; the major effect being to introduce a finite time τ beyond which classical steady wave analysis cannot be applied. Autocatalytic schemes have previously been applied for models of flame studies precisely to overcome this problem

We apply the 'pool chemical approximation' to the precursor P, assuming its (large) concentration remains constant at the initial value p_0 throughout. The governing reaction–diffusion equations for the three intermediate species then become

$$\partial a/\partial t' = D_A \nabla^2 a + k_0 p_0 c - k_1 a b^2, \tag{2a}$$

$$\partial b/\partial t' = D_B \nabla^2 b + k_1 a b^2 - k_2 b, \tag{2b}$$

$$\partial c/\partial t' = D_C \nabla^2 c + k_2 b - k_3 c. \tag{2c}$$

The boundary conditions and initial conditions of particular interest will be

$$a = a_1, \quad b = \begin{cases} b_0 g(r'), & |r'| < l, \\ 0, & |r'| > l, \end{cases} \quad c = 0 \text{ at } t' = 0, r' > 0, \tag{2d}$$

$$\partial a/\partial r' = \partial b/\partial r' = \partial c/\partial r' = 0 \quad \text{for} \quad r' = 0 \quad \text{and} \quad r' \to \infty \quad \text{for all } t. \tag{2e}$$

Equations (2) are made dimensionless, following Merkin *et al.* (1987*a*, *b*), by introducing the scalings

$$x = (k_1/k_2)^{\frac{1}{2}} a, \quad y = (k_1/k_2)^{\frac{1}{2}} b, \quad z = (k_1/k_2)^{\frac{1}{2}} c, \quad t = k_2 t'$$

We also assume equal diffusion coefficients and scale the length with $r = r'(k_2/D)^{\frac{1}{2}}$, to give

$$\partial x/\partial t = \nabla^2 x + \mu z - x y^2, \tag{3a}$$

$$\partial y/\partial t = \nabla^2 y + x y^2 - y, \tag{3b}$$

$$\partial z/\partial t = \nabla^2 z + y - \gamma z, \tag{3c}$$

subject to

$$x = x_1, \quad y = \begin{cases} y_0 g(r), & |r| < \sigma, \\ 0, & |r| > \sigma, \end{cases} \quad z = 0 \quad (t = 0, r > 0), \tag{3d}$$

$$\partial x/\partial r = \partial y/\partial r = \partial z/\partial r = 0 \quad (t > 0; r = 0 \quad \text{and} \quad r \to \infty), \tag{3e}$$

where the dimensionless parameters μ and γ are given by

$$\mu = (k_0 p_0)/k_2 \quad \text{and} \quad \gamma = k_3/k_2,$$

with $\mu > 0$ and $\gamma > 0$, $y_0 = (k_1/k_2)^{\frac{1}{2}} b_0$, $\sigma = l(k_2/D)^{\frac{1}{2}}$ and the initial input function $g(r)$ is positive and continuous on $|r| < \sigma$ with a maximum value of unity. The assumption of equal diffusion coefficients is realistic for the situations of interest when all chemical species have comparable molecular size. However, there are cases for example in the biochemical context where this is not the case and the diffusion coefficients can differ by many order of magnitude. This case has been examined in detail for a related chemical model by Billingham & Needham (1991*a*, *b*).

2. Well-stirred model

In all our previous studies of reaction–diffusion phenomena, experience has shown that a necessary prerequisite for efficient progress is the understanding of the behaviour of the corresponding 'well-stirred' ordinary differential equation (ODE)

PHILOSOPHICAL TRANSACTIONS OF THE ROYAL SOCIETY A MATHEMATICAL, PHYSICAL & ENGINEERING SCIENCES

system. Consequently, we begin here by examining the model in a continuously stirred, (but closed) rector, where equations (3) reduce to

$$\mathrm{d}x/\mathrm{d}t = \mu z - xy^2, \tag{4a}$$

$$\mathrm{d}y/\mathrm{d}t = xy^2 - y, \tag{4b}$$

$$\mathrm{d}z/\mathrm{d}t = y - \gamma z. \tag{4c}$$

On adding equation (4*a*–*c*), we obtain

$$\mathrm{d}x/\mathrm{d}t + \mathrm{d}y/\mathrm{d}t + \mathrm{d}z/\mathrm{d}t = (\mu - \gamma)\, z. \tag{5}$$

This leads to three distinct cases:

(*a*) $\mu > \gamma$, the 'expanding' case;
(*b*) $\mu < \gamma$, the 'contracting' case;
(*c*) $\mu = \gamma$, the 'reduced' case.

The terminology expanding or contracting refers to the total concentration of the intermediate species $x+y+z$ which increases or decreases with time respectively.

Considering the reduced case further, equation (5) becomes

$$\mathrm{d}x/\mathrm{d}t + \mathrm{d}y/\mathrm{d}t + \mathrm{d}z/\mathrm{d}t = 0,$$

which, on integration, gives

$$x + y + z = c_0, \tag{6}$$

where the positive constant c_0 represents the total initial concentration of the intermediate species A, B and C. Then, writing $z = c_0 - (x+y)$, equation (4*a*–*c*) reduces to the two-variable, two-parameter set

$$\mathrm{d}x/\mathrm{d}t = \mu(c_0 - x - y) - xy^2, \tag{7a}$$

$$\mathrm{d}y/\mathrm{d}t = xy^2 - y. \tag{7b}$$

We start by considering this reduced, two dimensional system (7) in some detail. Here, we find the possibility of multiple stationary states and of Hopf bifurcations, giving rise to both stable and unstable limit cycles. This oscillatory behaviour is found to break up via homoclinic orbit formation, the curve of which in parameter space arises from a double zero eigenvalue (DZE) point (Gray & Roberts 1988).

A detailed understanding of the reduced case then enables us to gain a clearer insight into the behaviour of the general (expanding and contracting) cases. We analyse these, both for when $|\mu - \gamma|$ is small and when $|\mu - \gamma|$ is of $O(1)$. In the former case, regions of oscillatory behaviour can be identified: oscillatory evolution develops spontaneously, but exists only for finite time periods. In the latter case, periods of oscillatory behaviour can be initiated only for the contracting system and then only in the limiting case when c_0 is large and with μ and γ both small, of $O(c_0^{-1})$. In all cases, none of the complex dynamical behaviour reported by Peng *et al.* (1990) is observed.

3. The reduced case, $\mu = \gamma$

(*a*) *Stationary states and local stability analysis*

Here we consider the two-parameter system given by equation (7*a*, *b*). These have a 'no reaction' stationary state solution corresponding to each reaction rate term becoming zero with

$$x_{\mathrm{ss}} = c_0, \quad y_{\mathrm{ss}} = 0 \tag{8a}$$

PHILOSOPHICAL TRANSACTIONS OF THE ROYAL SOCIETY A MATHEMATICAL, PHYSICAL & ENGINEERING SCIENCES

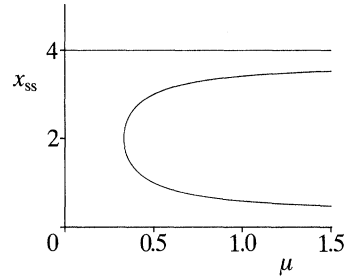

Figure 1. The dependence of the stationary-state concentration x_{ss} on the parameter μ for the reduced case with $c_0 = 4$ showing three branches: the solution $x_{ss} = c_0$ exists for all μ, whereas the two solutions given by equation (10) exist for $\mu \geqslant 4/(c_0^2-4) = \frac{1}{3}$.

for all parameter values. The stability of this solution is determined from the characteristic equation and governed by the eigenvalues λ given by

$$\lambda^2+(\mu+1)\lambda+\mu = 0, \tag{8b}$$

giving $\lambda = -\mu, -1$. These are both real and negative for all acceptable μ and hence this stationary state is always a stable node.

There are two further stationary states given by $x_{ss}\, y_{ss} = 1$, from equation (7*b*), with then

$$(\mu+1)\, y_{ss}^2-\mu c_0\, y_{ss}+\mu = 0, \tag{9}$$

giving

$$x_{ss} = (1/2\mu)\{\mu c_0-[\mu^2 c_0^2-4\mu(\mu+1)]^{\frac{1}{2}}\}, \quad y_{ss} = [1/2(\mu+1)]\{\mu c_0+[\mu^2 c_0^2-4\mu(\mu+1)]^{\frac{1}{2}}\}, \tag{10a}$$

$$x_{ss} = (1/2\mu)\{\mu c_0+[\mu^2 c_0^2-4\mu(\mu+1)]^{\frac{1}{2}}\}, \quad y_{ss} = [1/2(\mu+1)]\{\mu c_0-[\mu^2 c_0^2-4\mu(\mu+1)]^{\frac{1}{2}}\}, \tag{10b}$$

provided $c_0^2 \geqslant 4(\mu+1)/\mu$. From this, we require $\mu \geqslant 4/(c_0^2-4)$ and hence a necessary condition for the existence of this pair of stationary states is $c_0 > 2$. A graph of the stationary states x_{ss} as a function of μ for $c_0 = 4$ is shown in figure 1. Note that from (10*a*) $x_{ss} \to \frac{1}{2}\{c_0-[c_0^2-4]^{\frac{1}{2}}\} > 0$ and from (10*b*) $x_{ss} \to \frac{1}{2}\{c_0+[c_0^2-4]^{\frac{1}{2}}\} < c_0$ as $\mu \to \infty$.

The eigenvalues for stationary states (10*a*) and (10*b*) are given by the usual characteristic equation

$$\lambda^2-Tr\,\lambda+D = 0, \tag{11}$$

where $Tr = 1-\mu-y_{ss}^2$ and $D = (\mu+1)\, y_{ss}^2-\mu$ are the trace and determinant respectively of the jacobian matrix evaluated at the stationary states. Using equation (9), we have $D = \mu(c_0\, y_{ss}-2)$ and hence for stationary state (10*a*), where $y_{ss} > \mu c_0/2(\mu+1)$, then $D > \mu[\mu c_0^2-4(\mu+1)]/2(\mu+1) > 0$, from the condition for the existence of these 'non-zero' states.

For stationary state (10*b*), we find

$$D = [1/2(\mu+1)]\,[\mu^2 c_0^2-4\mu(\mu+1)]^{\frac{1}{2}}\{[\mu^2 c_0^2-4\mu(\mu+1)]^{\frac{1}{2}}-\mu c_0\} < 0.$$

Thus, it follows that stationary state (10*b*) is a saddle point for all $\mu > 4/(c_0^2-4)$. The two stationary states (10*a*) and (10*b*) merge at a saddle-node bifurcation with $\mu = 4/(c_0^2-4)$ or, equivalently, $c_0^2 = 4(\mu+1)/\mu$.

Stationary state (10*a*) has $D > 0$ for $\mu > 4/(c_0^2-4)$, so its stability will be

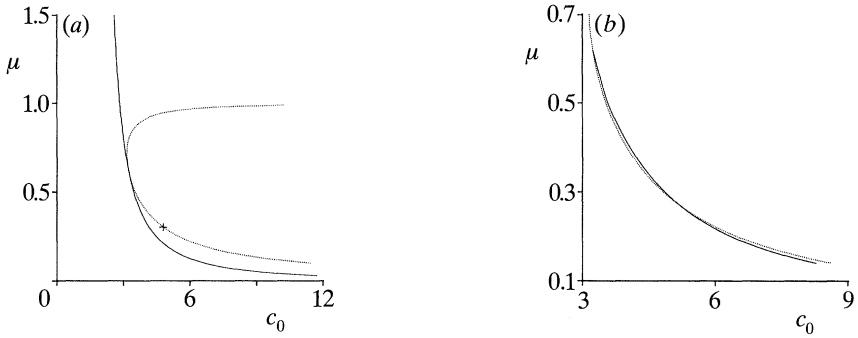

Figure 2. Loci of bifurcation points in the $c_0-\mu$ parameter plane: (*a*) saddle-node points (solid curve) and Hopf points (lower branch of broken curve) emerging from a double zero eigenvalue point – the Hopf bifurcation changes from subcritical to supercritical at the point +; (*b*) detail of Hopf locus and curve of homoclinic orbits, showing apparent crossing.

determined by the trace. In particular, there will be a point of Hopf bifurcation for $Tr = 0$ (subject to certain other qualifications). The condition $Tr = 0$ is satisfied with

$$\mu + y_{ss}^2 - 1 = 0, \tag{12a}$$

which, together with equation (9), gives a parametric representation of the Hopf curve. Substituting for y_{ss}, we obtain

$$c_0 = (1+\mu-\mu^2)/\mu[1-\mu]^{\frac{1}{2}}. \tag{12b}$$

Substituting the condition $c_0^2 = 4(\mu+1)/\mu$ into equation (12*b*), gives the condition for a double zero eigenvalue (i.e. at $Tr = D = 0$ so $\lambda = 0, 0$), at

$$\mu = \tfrac{1}{2}(\sqrt{5}-1), \quad c_0 = 1+\sqrt{5}. \tag{12c}$$

Thus it follows that Hopf bifurcation points lie on the locus described by equation (12*b*) for $\mu < \frac{1}{2}(\sqrt{5}-1)\,(\approx 0.618)$ and $c_0 > 1+\sqrt{5}(\approx 3.2361)$.

(*b*) *Stability of emerging limit cycle and degenerate bifurcation points*

The stability of the limit cycle emerging from the Hopf bifurcation was determined using the numerical package BIFOR2 (Hassard *et al.* 1980). This converged rapidly as the exact Hopf point is known from above and a systematic search with decreasing μ could readily be undertaken. A degenerate Hopf bifurcation point was located at $\mu = \mu^* = 0.3027$, $c_0 = c_0^* = 4.7912$. For $\mu > \mu^*$ ($c_0 < c_0^*$) the Hopf bifurcation described by equation (12*b*) is subcritical, giving rise to an unstable limit cycle, whilst for $\mu < \mu^*(c_0 > c_0^*)$ the bifurcation is supercritical and a stable limit cycle emerges.

The emerging limit cycles were followed numerically using essentially the same shooting method described by Forbes (1990; Forbes & Holmes 1990). This method has the added advantage of allowing the stability of the limit cycle to be determined by the calculation of the corresponding Floquet multipliers. The limit cycles were followed with increasing amplitude until their extinction at a homoclinic orbit arising from the saddle-node point. The homoclinic orbit was located using the method described in Kaas-Petersen & Scott (1988) and its locus in the parameter plane locus was similarly determined by repeating the calculations for a variety of c_0.

These various bifurcation loci are indicated in figure 2*a*, *b*. Figure 2*a* shows the saddle-node curve specified by $D = 0$, $\mu = 4/(c_0^2-4)$ and the Hopf bifurcation locus

PHILOSOPHICAL TRANSACTIONS OF THE ROYAL SOCIETY A MATHEMATICAL, PHYSICAL & ENGINEERING SCIENCES

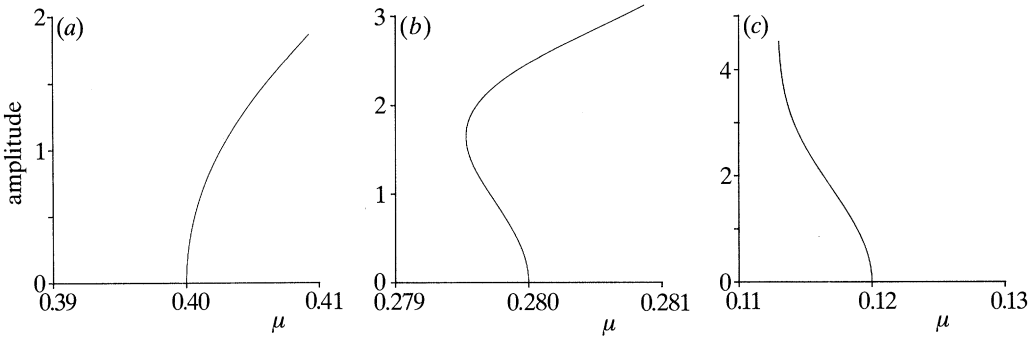

Figure 3. The development of oscillatory amplitude with the parameter μ: (*a*) $c_0 = 4.00208$, an unstable limit cycle emerges at $\mu^* = 0.4$ and grows for increasing μ, terminating at a homoclinic bifurcation; (*b*) $c_0 = 5.05750$, a stable limit cycle emerges at $\mu^* = 0.28$ and grows at first as μ decreases: the turning point in the locus corresponds to a loss of stability for the limit cycle, and the unstable cycle grows as μ increases again, terminating in a homoclinic orbit for $\mu > \mu^*$; (*c*) $c_0 = 9.82145$, a stable limit cycle emerges at $\mu^* = 0.12$ and grows as μ decreases: the turning point before the homoclinic orbit formation, at $\mu < \mu^*$, is not visible on this scale.

(broken curve) given by equation (12*b*). This latter meets the saddle-node curve at the DZE point given by (12*c*). It is the lower branch of this curve that corresponds to Hopf bifurcation points (these lie on the lowest branch of stationary states in figure 1). The degenerate Hopf bifurcation point is also marked on this curve. The upper branch of the $Tr = 0$ curve corresponds to this condition being satisfied for a stationary state lying on the intermediate, saddle branch in figure 1. This portion of the curve does not correspond to any bifurcation in the system, but its position relative to the locus of homoclinic orbits is of some relevance. Figure 2*b* shows on an expanded scale the detail of the relative positions of the Hopf bifurcation and homoclinic orbit loci. Both emerge from the DZE point (12*c*). Initially, the homoclinic orbit curve lies above the Hopf locus (i.e. the unstable limit cycle that emerge from the Hopf point grow as μ increases and forms its homoclinic orbit at some larger μ). This station is shown in figure 3*a* for the representative case $c_0 = 4.00208$: the Hopf bifurcation occurs at $\mu = 0.4$.

The homoclinic curve remains above the Hopf locus as we pass through the degenerate Hopf point (μ^*, c_0^*). For larger c_0 (lower μ), the Hopf bifurcation now yields a stable limit cycle that grows as μ decreases from the Hopf point. The homoclinic orbit, however, is still formed at some μ greater than the Hopf point. There must, therefore, be a turning point in the limit cycle locus at some point, as indicated in figure 3*b* for the case $c_0 = 5.05750$, for which the Hopf bifurcation occurs at $\mu = 0.28$. As the limit cycle passes round the turning point, it changes stability, becoming unstable. Thus, for values of μ between this turning point and the Hopf point the system has two limit cycle solutions around the (unstable) lowest stationary state. The smaller cycle (that with lowest amplitude) is stable, but this is surrounded by an unstable limit cycle. The unstable cycle grows in amplitude as μ increases, as before, and terminates in its homoclinic orbit.

At yet larger values for the total intermediate initial concentration, c_0, the Hopf and homoclinic curves appear to cross. Thus, the homoclinic orbit occurs at lower values of μ than the Hopf point. Such a situation is shown in figure 3*c* for $c_0 = 9.82145$. A stable limit cycle emerges at $\mu = 0.12$ and grows as μ decreases. There is, in fact, a change in stability of the limit cycle at the highest amplitude, just before

PHILOSOPHICAL TRANSACTIONS OF THE ROYAL SOCIETY A MATHEMATICAL, PHYSICAL & ENGINEERING SCIENCES

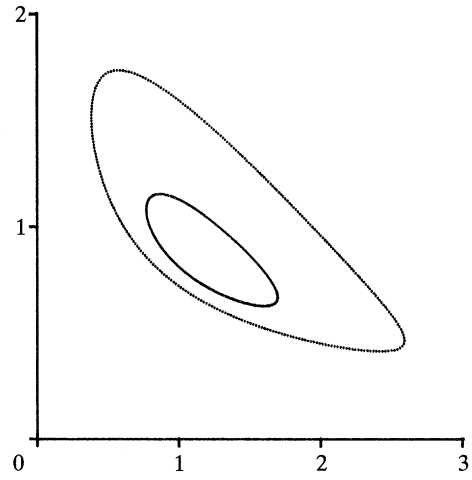

Figure 4. Example limit cycles for $\mu = 0.27974$, $c_0 = 5.05799$.

homoclinic orbit formation, although this is not easily seen from the scale of the figure. Figure 4 shows a representative pair of coexisting limit cycle for $\mu = 0.2797$ and $c_0 = 5.05799$: the unstable limit cycle surrounds the smaller, stable cycle.

(c) *Asymptotic analysis for large* c_0

The behaviour of the homoclinic orbit curve for large c_0 (and small μ) can be determined if we consider the initial-value problem given by equation (7 *a*, *b*) subject to

$$x(0) = 0, \quad y(0) = c_0, \quad \bar{\mu} = \mu c_0, \quad c_0 \gg 1, \tag{13}$$

where $\bar{\mu}$ is of $O(1)$. To start the solution we note that there is an initial region where t is of $O(1)$ and where x is of $O(c_0^{-2})$ and y is of $O(c_0)$. This suggests putting

$$x = c_0^{-2} X, \quad y = c_0 Y. \tag{14a}$$

Equations (7) then become

$$\bar{\mu}(1-Y) - XY^2 - (\bar{\mu}/c_0^3) X = (1/c_0^2)\, \mathrm{d}X/\mathrm{d}t, \tag{14b}$$

$$\mathrm{d}Y/\mathrm{d}t + Y = (1/c_0) XY^2, \tag{14c}$$

subject to the initial conditions

$$X(0) = 0, \quad Y(0) = 1. \tag{14d}$$

Equation (14 *c*) suggests looking for a solution in the form of an expansion

$$X(t; c_0) = X_0(t) + c_0^{-1} X_1(t) + \ldots, \quad Y(t; c_0) = Y_0(t) + c_0^{-1} Y_1(t) + \ldots. \tag{15}$$

Substituting (15) into equation (14 *b*, *c*) and equating terms of like power in c_0, we obtain after a little manipulation

$$Y_0 = \mathrm{e}^{-t}, \qquad X_0 = \bar{\mu}\, \mathrm{e}^t (\mathrm{e}^t - 1), \tag{16a}$$

$$Y_1 = \bar{\mu}(1 - \mathrm{e}^{-t} - t\, \mathrm{e}^{-t}), \quad X_1 = -\bar{\mu}^2\, \mathrm{e}^{2t} (2\mathrm{e}^t - 1)\, (1 - t\, \mathrm{e}^{-t} - \mathrm{e}^{-t}), \tag{16b}$$

These forms show that expansion (15) becomes non-uniform when t is of $O(\ln c_0)$, with then x and y both being of $O(1)$.

To continue the solution, we put $t = \ln(c_0/\bar{\mu}) + \bar{t}$ and leave x and y unscaled. Then, with $\mu = \bar{\mu}c_0^{-1}$, the equation satisfied by x and y are, at leading order

$$\mathrm{d}x/\mathrm{d}\bar{t} = \bar{\mu} - xy^2, \tag{17a}$$

$$\mathrm{d}y/\mathrm{d}\bar{t} = xy^2 - y, \tag{17b}$$

with, from equation (16),

$$x \sim \frac{\mathrm{e}^{2\bar{t}}}{\bar{\mu}} - \frac{2\mathrm{e}^{3\bar{t}}}{\bar{\mu}} + \ldots, \quad y \sim \bar{\mu}\mathrm{e}^{-\bar{t}} + \bar{\mu} + \ldots \quad \text{as} \quad \bar{t} \to -\infty \tag{17c}$$

Now, equation (17*a*, *b*) are those of the original autocatalator model (Merkin *et al.* 1986), from which it follows that they possess one (finite) stationary state $(\bar{\mu}^{-1}, \bar{\mu})$. This is stable for $\bar{\mu} > 1$, with a Hopf bifurcation at $\bar{\mu} = 1$ leading to a stable limit cycle that grows for $\bar{\mu} < 1$. The oscillatory behaviour breaks down at $\bar{\mu} = \bar{\mu}_c \approx 0.900\,32$ through the formation of a heteroclinic orbit from points at infinity. For $\bar{\mu} < \bar{\mu}_c$, the solution becomes unbounded, with $x \sim \bar{\mu}\bar{t}$, $y \to 0$ as $\bar{t} \to \infty$. This implies that for $\bar{\mu} > 1$, to leading order, $x \to \bar{\mu}^{-1}$, $y \to \bar{\mu}$ as $\bar{t} \to \infty$. which is the asymptotic form of stationary state (10*a*) in this limit. For $\bar{\mu}_c < \bar{\mu} < 1$, the solution approaches a stable limit cycle as $\bar{t} \to \infty$. For $\bar{\mu} < \bar{\mu}_c$, the solution becomes unbounded on this timescale and a further, outer region is required in which t is of $O(c_0)$. To complete this case we then put

$$x = c_0\bar{X}, \quad \bar{t} = c_0\tau \tag{18a}$$

and, with y exponentially small, we then obtain

$$\mathrm{d}\bar{X}/\mathrm{d}\tau = \bar{\mu}(1 - \bar{X}), \quad \text{with} \quad \bar{X} \sim \bar{\mu}\tau + \ldots, \tau \ll 1, \tag{18b}$$

which has the solution

$$\bar{X} = (1 - \mathrm{e}^{-\bar{\mu}\tau}). \tag{18c}$$

So that, finally, with $\bar{\mu} < \bar{\mu}_c$, x becomes large with

$$x \to c_0, \quad y \to 0. \tag{18d}$$

The above analysis shows that for $c_0 \gg 1$, the Hopf bifurcation and homoclinic orbit loci should become parallel for c_0 large, being given by $c_0^{-1} + \ldots$ and $\bar{\mu}_c c_0^{-1} + \ldots$ respectively.

This behaviour can be seen in figure 2*b* and from figure 3*c* in which the development of the amplitude with μ closely resembles that given in Merkin *et al.* (1986). The values of the Hopf bifurcation and the homoclinic point are in reasonable agreement with the above forms even for this value of c_0 (the error is *ca.* 0.02 in each case, with $\mu \sim 0.1$).

As a check on the above theory for $c_0 \gg 1$, we integrated equations (7) numerically taking $c_0 = 50$ with representative values of μ, namely $\mu = 0.06$ ($\bar{\mu} = 3.0$), $\mu = 0.019$ ($\bar{\mu} = 0.95$) and $\mu = 0.012$ ($\bar{\mu} = 0.6$). The results are shown in figure 5. With $\mu = 0.06$, figure 5*a*, we see that (x, y) rapidly approaches the stationary state $(\bar{\mu}^{-1}, \bar{\mu})$ as required. For $\mu = 0.019$ there is a sustained oscillatory response, figure 5*b*, in both x and y and with $\mu = 0.012$, figure 5*c*, the asymptotic values (18*d*) are approached, with $y \to 0$ rapidly and $x \to c_0$ over a much longer timescale.

The detailed information obtained above for this reduced case, $\mu = \gamma$, provides a framework against which to discuss the general case $\mu \neq \gamma$. We start this discussion by considering the case $|\mu - \gamma| \ll 1$ first.

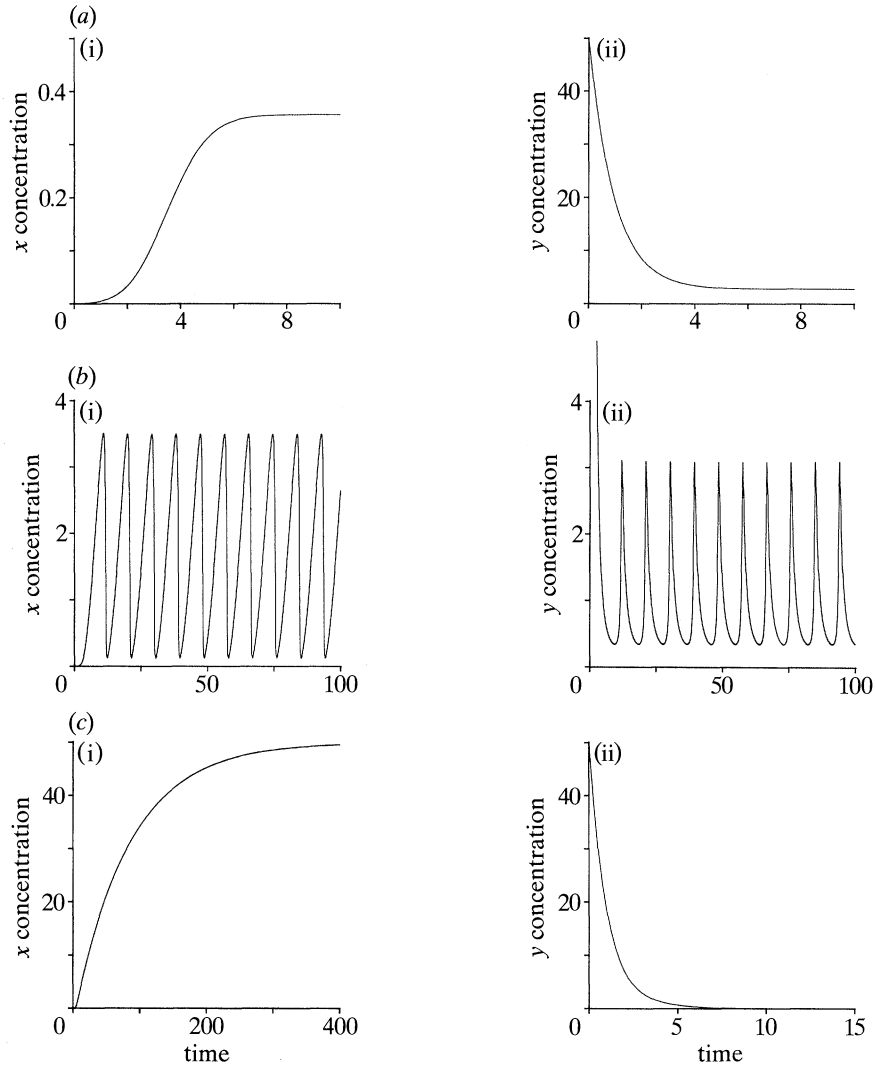

Figure 5. The behaviour for the reduced case with large initial concentration of autocatalyst ($c_0 = 50$) showing the Hopf and homoclinic bifurcation structure as μ varies: (*a*) $\mu = 0.06$ ($\bar{\mu} > 1$), showing approach to stable 'non-zero' state; (*b*) $\mu = 0.019$ ($\bar{\mu}_c < \bar{\mu} < 1$) showing stable oscillatory response; (*c*) $\mu = 0.012$ ($\bar{\mu} < \bar{\mu}_c$) showing asymptotic approach to 'zero reaction' state.

4. General case, $|\mu-\gamma|$ small

Equation (5) suggests that to interpret the full scheme it is appropriate to use a change of variables, from (x, y, z) to (x, y, ξ), where $\xi = x+y+z$. Equations (4) then become

$$\mathrm{d}x/\mathrm{d}t = \mu(\xi-x-y)-xy^2, \tag{19a}$$

$$\mathrm{d}y/\mathrm{d}t = xy^2-y, \tag{19b}$$

$$\mathrm{d}\xi/\mathrm{d}t = \epsilon(\xi-x-y), \tag{19c}$$

where $\epsilon = \mu-\gamma$.

To integrate equations (19) we also need to specify the initial conditions. A property of such autocatalytic schemes is that reaction does not begin spontaneously

if no autocatalyst is present initially. If, however, some B is added to the initial P, species C will be produced via step (1*c*) and this then can catalyse the production of A via step (1*a*). To be explicit, then, we assume initial conditions of the form such that only intermediate B is present (in addition to the precursor), i.e. we take

$$x(0) = 0, \quad y(0) = c_0, \quad \xi(0) = c_0 \tag{20}$$

so the initial concentration c_0 can be identified with the constant of integration used previously in the reduced case.

(*a*) *The contracting case*, $\mu < \gamma$

The contracting case, with $\mu < \gamma$, corresponds to $\epsilon < 0$ in equation (19*c*). We start our analysis by assuming $|\epsilon| \ll 1$. Equations (19) were integrated numerically subject to initial conditions (20) using a standard Runge–Kutta method, for a range of values of μ and c_0. The values of these parameters were chosen so as to investigate the behaviour for this case in direct comparison with that in the different regions of the $\mu - c_0$ plane of the reduced case, figure 2*a*, *b*.

(i) *Computed examples*

The parameter set $\mu = 0.50$, $c_0 = 3.0$ and $\epsilon = -0.01$ corresponds to conditions below the saddle-node curve in figure 2*a* for the reduced case, so that only the 'no reaction' stationary state (8*a*) exists for that system. The evolution of the present system is shown in figure 6*a*, and shows a rapid approach to this same stationary state.

With $\mu = 0.80$, $c_0 = 6.0$ the reduced system shows multistability but lies well above the Hopf bifurcation and homoclinic orbit curves in figure 2*b*. With, again, $\epsilon = -0.01$, the resulting evolution of the contracting case, figure 6*b*, shows a definite three time-region structure before the final stationary-state is attained.

Finally, we took $\mu = 0.12$ and $c_0 = 10.0$. This corresponds to the region just above the Hopf bifurcation curve and with $\mu < \mu^*(c_0 > c_0^*)$ so that the reduced system has a stable limit cycle co-existing with the 'no reaction' state. To distinguish fully the structure of the solution in this case, it proved necessary to employ a value of ϵ smaller than that used in the previous cases. We took $\epsilon = -0.001$ and the resulting evolution is shown in figure 6*c*. Here, we can see the rapid onset of oscillatory behaviour, first decreasing in amplitude but then increasing before an abrupt change towards the final stationary state is reached. This structure is brought out even more spectacularly in figure 6*d*, for which a value of the 'decay' parameter $\epsilon = -0.0001$ was taken. In this case, the oscillatory behaviour dies away to almost zero amplitude for $100 < t < 350$ before increasing again. There is again a three time-region structure to the solution.

(ii) *Asymptotic development*

To complete this discussion and to attempt to understand more clearly the nature of the results shown in figure 6, we obtain a solution of equations (19) subject to initial conditions (20) for $|\epsilon| \ll 1$. To do this we put $\delta = -\epsilon$, where $0 < \delta \ll 1$ and expand

$$\left.\begin{aligned} x(t;\mu,\delta) &= x_0(t) + \delta x_1(t) + \ldots, \\ y(t;\mu,\delta) &= y_0(t) + \delta y_1(t) + \ldots, \\ \xi(t;\mu,\delta) &= \xi_0(t) + \delta \xi_1(t) + \ldots, \end{aligned}\right\} \tag{21}$$

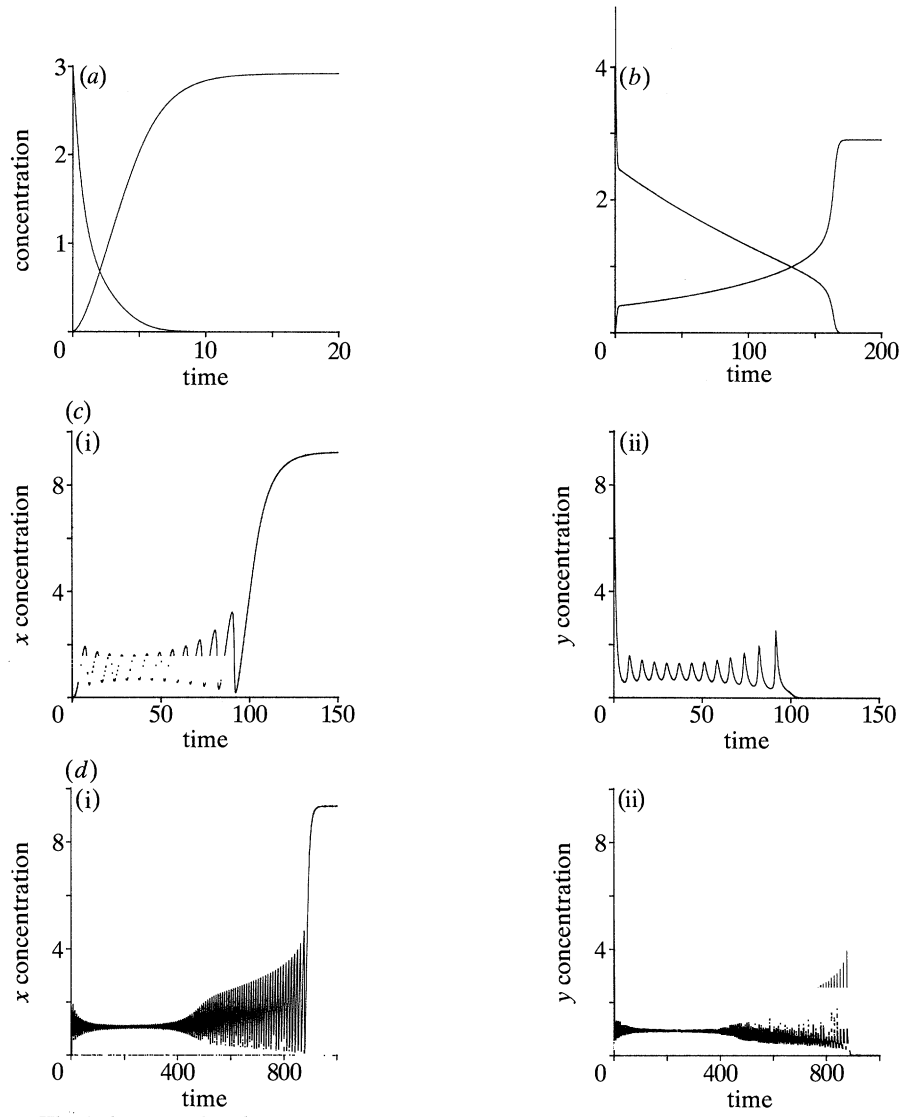

Figure 6. The behaviour for the 'contracting case', $\epsilon < 0$: (*a*) $\mu = 0.5$, $c_0 = 3.0$, $\epsilon = -0.01$, showing simple evolution to 'no reaction' state ($y \to 0$); (*b*) $\mu = 0.8$, $c_0 = 6.0$, $\epsilon = -0.01$ showing approach to quasi-steady non-zero state before rapid transition to vicinity of final concentrations; (*c*) $\mu = 0.12$, $c_0 = 10.0$, $\epsilon = -0.001$ showing approach to quasi-steady oscillatory solution followed by 'homoclinicity' and approach to final, steady concentrations; (*d*) as for (*c*) but with $\epsilon = -0.0001$ showing closer approach to quasi-steady, focal state and Hopf bifurcation structure.

and leave t unscaled. At leading order, we obtain

$$\mathrm{d}\xi_0/\mathrm{d}t = 0, \quad \text{so} \quad \xi_0 = c_0 \tag{22}$$

with then x_0 and y_0 satisfying the reduced two-variable scheme, given by equations (7) and discussed in the previous section.

Now (x_0, y_0) will approach a stable attractor for t large, which allows three possibilities: (x_0, y_0) may approach stationary state 8(*a*), stationary state (10*a*) (either directly as a stable node or via damped oscillations if this is a stable focus) or the limit cycle. The values of c_0 and μ determine which of these options is realized.

(iii) *Approach to 'zero reaction' state* (8*a*)

For $\mu < 4/(c_0^2-4)$, state (8*a*) is the only stable attractor available and so is approached as $t\to\infty$. With $\mu > 4/(c_0^2-4)$, stationary states (10*a*, *b*) also exist and the initial conditions start the solution in the basin of attraction of state (10*a*), if this is stable, or of the stable limit cycle surrounding this, if this state is unstable. Thus the system moves towards this as $t\to\infty$. If, however, state (10*a*) is stable but surrounded by an unstable limit cycle, our initial conditions typically lie outside the basin of attraction of this solution and so again tend to the stable state (8*a*).

At $O(\delta)$ we obtain the equations

$$\mathrm{d}x_1/\mathrm{d}t = -(\mu+y_0^2)\,x_1-(\mu+2x_0\,y_0)\,y_1+\mu\xi_1, \tag{23a}$$

$$\mathrm{d}y_1/\mathrm{d}t = (2x_0\,y_0-1)\,y_1+y_0^2\,x_1, \tag{23b}$$

$$\mathrm{d}\xi_1/\mathrm{d}t = -\xi_0+x_0+y_0. \tag{23c}$$

The main interest from equations (23) is the behaviour of the solution for large t. We take the case when (x_0, y_0) approaches the 'no reaction' state (8*a*) first. Consideration of the above equations shows then that

$$x_1\to c_1, \quad y_1\to 0, \quad \xi_1\to c_1 \quad \text{as} \quad t\to\infty \tag{24a}$$

or some constant c_1. In this case, the expansion (21) remains uniform for all t (and this is confirmed by the consideration of higher order terms), with then

$$x\to c_0+O(\delta), \quad y\to 0, \quad \xi\to c_0+O(\delta) \tag{24b}$$

as $t\to\infty$. This behaviour can be seen clearly in figure 6*a*.

(iv) *Approach to stable nodal state* (10*a*)

Next, consider the case when (x_0, y_0) approaches stationary state (10*a*) monotonically (stable node). Equation (23) now reveal that

$$\left.\begin{aligned} \xi_1 &\sim (x_{\mathrm{ss}}+y_{\mathrm{ss}}-c_0)\,t+c_2, \\ x_1 \sim \frac{\mu(x_{\mathrm{ss}}+y_{\mathrm{ss}}-c_0)\,t}{\mu-(\mu+1)\,y_{\mathrm{ss}}^2}+\ldots, &\quad y_1 \sim \frac{-\mu y_{\mathrm{ss}}^2(x_{\mathrm{ss}}+y_{\mathrm{ss}}-c_0)\,t}{\mu-(\mu+1)\,y_{\mathrm{ss}}^2}+\ldots, \end{aligned}\right\} \tag{25}$$

where x_{ss} and y_{ss} are given by equation (10*a*). Note that

$$x_{\mathrm{ss}}+y_{\mathrm{ss}}-c_0 = -[1/2\mu(\mu+1)]\,\{\mu c_0+[\mu^2c_0^2-4\mu(\mu+1)]^{\frac{1}{2}}\} < 0.$$

Equations (25) show that, in this case, expansion (21) becomes non-uniform on a timescale of $O(\delta^{-1})$ with x, y and ξ all of $O(1)$. A further time region is now required in which $\tau = \delta t$ is of $O(1)$. Substituting this new time into equations (19) and leaving x, y and ξ unscaled, we obtain at leading order

$$\mu(\xi-x-y)-xy^2 = 0, \tag{26a}$$

$$xy^2-y = 0, \tag{26b}$$

$$\mathrm{d}\xi/\mathrm{d}\tau = x+y-\xi, \tag{26c}$$

with, from matching to the previous time region,

$$x\sim x_{\mathrm{ss}}+O(\tau), \quad y\sim y_{\mathrm{ss}}+O(\tau), \quad \xi = c_0+O(\tau) \quad \text{as} \quad \tau\to 0. \tag{26d}$$

The solution of equation (26a, b) which matches with (26d) and is consistent with (10a) is

$$x = \{\mu\xi - [\mu^2\xi^2 - 4\mu(1+\mu)]^{\frac{1}{2}}\}/2\mu, \tag{27a}$$

$$y = \{\mu\xi + [\mu^2\xi^2 - 4\mu(1+\mu)]^{\frac{1}{2}}\}/2(\mu+1), \tag{27b}$$

with, then, equation (26c) becoming

$$\mathrm{d}\xi/\mathrm{d}\tau = -[1/2\mu(\mu+1)]\{\mu\xi + [\mu^2\xi^2 - 4\mu(1+\mu)]^{\frac{1}{2}}\} \tag{27c}$$

Equation (27c) has the solution, given implicitly by,

$$[\xi/8(\mu+1)]\{\mu\xi - [\mu^2\xi^2 - 4\mu(1+\mu)]^{\frac{1}{2}}\} - [c_0/8(\mu+1)]\{\mu c_0 - [\mu^2 c_0^2 - 4\mu(1+\mu)]^{\frac{1}{2}}\}$$
$$+ \tfrac{1}{2}\ln\left\{\frac{\mu\xi + [\mu^2\xi^2 - 4\mu(1+\mu)]^{\frac{1}{2}}}{\mu c_0 + [\mu^2 c_0^2 - 4\mu(1+\mu)]^{\frac{1}{2}}}\right\} + \frac{\tau}{2(\mu+1)} = 0. \tag{28a}$$

Now equation (28a) becomes singular as $\xi \to 2[(\mu+1)/\mu]^{\frac{1}{2}}$ and

$$\tau \to \tau_0 = 2(\mu+1)\left\{\frac{c_0}{8\mu(\mu+1)}\{\mu c_0 - [\mu^2 c_0^2 - 4\mu(1+\mu)]^{\frac{1}{2}}\}\right.$$
$$\left. - \tfrac{1}{2}\ln\left\{\frac{\mu c_0 + [\mu^2 c_0^2 - 4\mu(1+\mu)]^{\frac{1}{2}}}{2[\mu(\mu+1)]^{\frac{1}{2}}}\right\}\right\} \tag{28b}$$

with then, from equation (27a, b),

$$x \to [(\mu+1)/\mu]^{\frac{1}{2}}, \quad y \to [\mu/(\mu+1)]^{\frac{1}{2}}. \tag{28c}$$

A final time region is then required in which

$$t = \tau_0\,\delta^{-1} + \bar{t} \tag{29a}$$

and in which x, y and ξ are unscaled. The resulting equations, at leading order, are

$$\mathrm{d}\xi/\mathrm{d}t = 0, \quad \xi = 2[(\mu+1)/\mu]^{\frac{1}{2}} \tag{29b}$$

and then

$$\mathrm{d}x/\mathrm{d}t = \mu\{2[(\mu+1)/\mu]^{\frac{1}{2}} - x - y\} - xy^2, \tag{29c}$$

$$\mathrm{d}y/\mathrm{d}t = xy^2 - y. \tag{29d}$$

Consideration of the $O(\delta)$ terms in the solutions for the previous time region shows these to be of $O((\tau_0 - \tau)^{-1})$ as $\tau \to \tau_0$. This, in turn, leads to the initial conditions for x and y via (28c) as

$$x \sim [(\mu+1)/\mu]^{\frac{1}{2}} + O(\bar{t}^{-1}), \quad y \sim [\mu/(\mu+1)]^{\frac{1}{2}} + O(\bar{t}^{-1}) \tag{29e}$$

as $\bar{t} \to -\infty$.

Equations (29c, d) have two stationary states $(2[(\mu+1)/\mu]^{\frac{1}{2}}, 0)$ and $([(\mu+1)/\mu]^{\frac{1}{2}}, [\mu/(\mu+1)]^{\frac{1}{2}})$ and it is straightforward to show that the former of these is a stable node for all values of μ. However, the initial conditions (29e) start the solution close to the second of these stationary states whose stability we must therefore determine. For this, we need the centre manifold theorem (Verhulst 1990) as the linearized version of this equation has a zero eigenvalue, $\lambda_1 = 0$, with the associated eigenvector $\boldsymbol{e}_1 = (1, -\mu/(1+\mu))^{\mathrm{T}}$. The second eigenvalue $\lambda_2 = (1-\mu-\mu^2)/(\mu+1)$ with the corresponding eigenvector $\boldsymbol{e}_2 = (1, -1/(\mu+2))^{\mathrm{T}}$. For $\mu < \frac{1}{2}(\sqrt{5}-1)$, $\lambda_2 > 0$ and this stationary state is unstable. However, for $\mu > \frac{1}{2}(\sqrt{5}-1)$, $\lambda_2 < 0$ and further considerations are required.

The discussion above shows that for $\mu > \frac{1}{2}(\sqrt{5}-1)$, there is a unique one-dimensional invariant stable manifold which is locally tangent to $\boldsymbol{e}_2$, together with a one-dimensional centre manifold locally tangent to $\boldsymbol{e}_1$. An application of Carr's theorem then shows that all phase paths in the neighbourhood of $([(\mu+1)/\mu]^{\frac{1}{2}}, [\mu/(\mu+1)]^{\frac{1}{2}})$ contract rapidly onto this centre manifold. To determine the local form of this centre manifold, we have first to transform the variables from (x, y) to $(\bar{x}, \bar{y})$, where

$$x = [(\mu+1)/\mu]^{\frac{1}{2}} + \bar{x}, \quad y = [\mu/(\mu+1)]^{\frac{1}{2}} + \bar{y}$$

with then

$$X = \bar{x} + (\mu+2)\,\bar{y}, \qquad Y = [\mu/(\mu+1)]\,\bar{x} + \bar{y}.$$

This puts the equations into the appropriate form for calculating the centre manifold, which we find, after a little calculation, to be given by

$$Y = [-\mu^2/(\mu^2+\mu-1)^3][\mu/(\mu+1)]^{\frac{1}{2}}X^2 + O(X^3). \tag{30a}$$

The dynamics on the centre manifold are then given by

$$\mathrm{d}X/\mathrm{d}\bar{t} = [-3\mu(\mu+1)^2/(\mu^2+\mu-1)^2][\mu/(\mu+1)]^{\frac{1}{2}}X^2 + O(X^3). \tag{30b}$$

This then shows that the solution paths approach the stationary state on the centre manifold (30*a*) in $X > 0$, whilst they leave it in $X < 0$. This, together with the stable manifold tangential to $\boldsymbol{e}_2$ gives a saddle-node appearance to the stationary state $([(\mu+1)/\mu]^{\frac{1}{2}}, [\mu/(\mu+1)]^{\frac{1}{2}})$. From this, it follows that this state is unstable to perturbations of the form given by the initial conditions (29*e*), with the solution to equation (29*c*, *d*) then having

$$x \to 2[(\mu+1)/\mu]^{\frac{1}{2}}, \quad y \to 0 \quad \text{as} \quad t \to \infty \tag{31}$$

on the timescale with $\bar{t}$ of $O(1)$.

This is the situation for the results shown in figure 6*b*. The three distinct timescales can be seen clearly. There is an initial adjustment on an $O(1)$ timescale to the values given by equations (26*d*) and (27*a b*), followed by a slower change on an $O(\delta^{-1})$ timescale to $\tau = \tau_0$, as given by equation (28*b*), with a final region in which the final forms given by equation (31) are rapidly attained.

(v) *Approach to stable focal state* (10*a*) *or to stable limit cycle*

Next, we consider the case when the solution in the initial time region approaches either the stationary state (10*a*) through a damped oscillatory response (if it is stable) or the stable limit cycle if the stationary state is unstable. Here it is more appropriate to use a two-timescale analysis, with a fast time t and a slow time $\tau = \delta t$. This leads to the equations

$$\partial x/\partial t + \delta\,\partial x/\partial \tau = \mu(\xi - x - y) - xy^2, \tag{32a}$$

$$\partial y/\partial t + \delta\,\partial y/\partial \tau = xy^2 - y, \tag{32b}$$

$$\partial \xi/\partial t + \delta\,\partial \xi/\partial \tau = -\delta(\xi - x - y). \tag{32c}$$

We now expand

$$x = x_0 + \delta x_1 + \ldots, \quad y = y_0 + \delta y_1 + \ldots, \quad \xi = \xi_0 + \delta \xi_1. \tag{33}$$

At leading order, we have

$$\partial \xi_0/\partial t = 0, \tag{34a}$$

which has the solution

$$\xi_0 = A_0(\tau), \quad A_0(0) = c_0 \tag{34b}$$

with equation (32a, b) then giving

$$\partial x_0/\partial t = \mu[A_0(\tau) - x_0 - y_0] - x_0 y_0^2, \tag{35a}$$

$$\partial y_0/\partial t = x_0 y_0^2 - y_0. \tag{35b}$$

At $O(\delta)$ we obtain

$$\partial \xi_1/\partial t + \partial A_0/\partial \tau = -A_0 + (x_0 + y_0), \quad \xi_1(0) = 0. \tag{36a}$$

Equation (36a) leads to secular terms at this order and, hence, would render expansion (33) non-uniform unless $A_0(\tau)$ satisfies the equation

$$\mathrm{d}A_0/\mathrm{d}\tau + A_0 = 0, \tag{36b}$$

which has the solution

$$A_0 = c_0 \mathrm{e}^{-\tau}. \tag{36c}$$

We are now in a position to interpret the solution in this case. Equation (36c) shows that A_0 decreases slowly, on an $O(\delta^{-1})$ timescale, which is equivalent to quasi-statically reducing the effective value of c_0 in the reduced case and hence moving (in figure 2a) from a region of stable focal behaviour by crossing the Hopf bifurcation curve (which in this case gives rise to the birth of a stable limit cycle). Thus there is an initial period in which the quasi-steady stationary rates are attained through a damped oscillatory response (these have a frequency on the t timescale of $O(1)$). Thus for t sufficiently large with τ of $O(1)$

$$x_0 \sim \{\mu A_0 - [\mu^2 A_0^2 - 4\mu(\mu+1)]^{\frac{1}{2}}\}/2\mu, \quad y_0 \sim \{\mu A_0 + [\mu^2 A_0^2 - 4\mu(\mu+1)]^{\frac{1}{2}}\}/2(\mu+1). \tag{37}$$

The system undergoes an effective Hopf bifurcation at $\tau = \tau_c$ where, from equation (12b)

$$A(\tau_c) = A_c = (1+\mu-\mu^2)/\mu(1-\mu)^{\frac{1}{2}} < c_0. \tag{38}$$

For $\tau > \tau_c$, the solution follows essentially the same behaviour as that described in Merkin *et al.* (1986). The quasi-steady stationary state (37) becomes unstable and there is a region of oscillation about this solution, with growing amplitude and period, before the final break-up via an effective homoclinic orbit bifurcation, with finally, to leading order

$$x \to A_c, \quad y \to 0 \tag{39}$$

On a timescale for t of $\tau_c + O(1)$. When we start in the parameter range where the initial attractor is already the stable limit cycle, the situation is similar, except that now the period of decaying oscillations is absent and we proceed directly to the homoclinic orbit bifurcation with, again, equation (39) giving the final asymptotic behaviour.

The situation in this case can clearly be seen in figure 6c, d. Here $A_c = 9.821\,45$ and, as predicted by equation (39), this is the final value of x. The initial region of damped oscillation followed by a quasi-static evolution are seen followed by the final region of growing oscillations.

5. The expanding case, $\mu < \gamma : \mu - \gamma \ll 1$

The expanding case arises when $\mu > \gamma$, corresponding to $\epsilon > 0$ in equations (19). We start by considering the solution for $\epsilon \ll 1$. This analysis follows closely that given in the previous section for $\epsilon < 0$. There is typically an initial time region in which t is of $O(1)$ and during which we expand x, y and ξ in a power series in ϵ. At

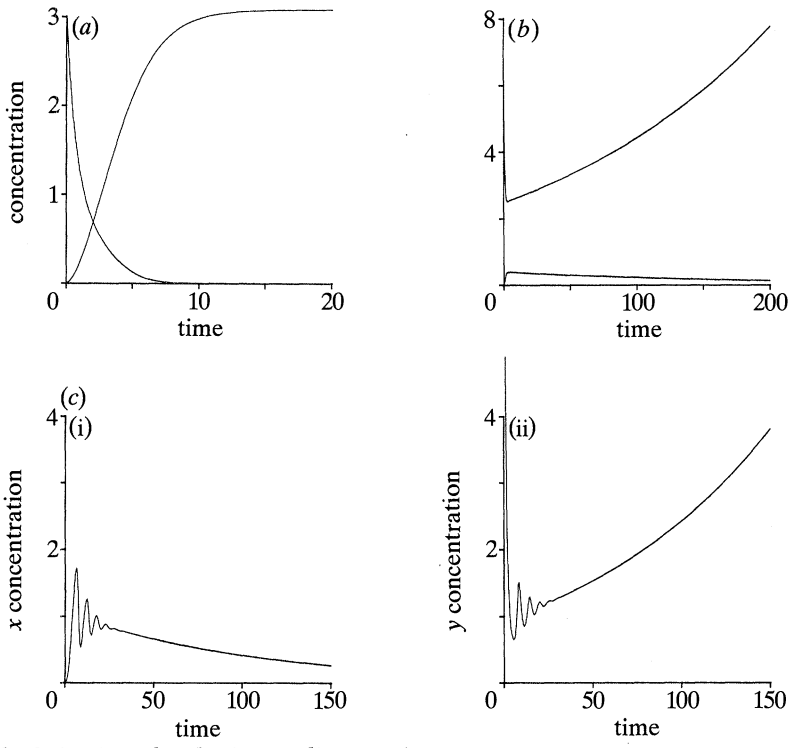

Figure 7. The behaviour for the 'expanding case', $\epsilon > 0$: (*a*) $\mu = 0.5$, $c_0 = 3.0$, $\epsilon = 0.01$, showing rapid evolution to 'no reaction' state ($y \to 0$); (*b*) $\mu = 0.8$, $c_0 = 6.0$, $\epsilon = 0.01$, system moves onto 'non-zero reaction' branch with x decreasing and y increasing quasi-statically; (*c*) $\mu = 0.12$, $c_0 = 10.0$, $\epsilon = 0.001$, showing an initial damped oscillatory motion onto the quasi-steady 'non-zero reaction' branch.

leading order we still find $\xi_0 = c_0$ with x and y still governed by equations (7) of the reduced system, with the three asymptotic limits as $t \to \infty$ still being possible. Again, if $\mu < 4/(c_0^2 - 4)$, the expansion in this region remains uniform with the large time behaviour given by equation (24*b*). This can be seen in the time series in figure 7*a* for the system with the same parameter values of that in figure 6*a* except than now $\epsilon > 0$.

With $\mu > 4/(c_0^2 - 4)$, the stable stationary state (10*a*) can be approached, with again the $O(\epsilon)$ terms rendering the expansion non-uniform on a timescale of $O(\epsilon^{-1})$. A further time region of $O(\epsilon^{-1})$ is required and with $\tau = \epsilon t$, the equation satisfied by ξ is, to leading order, now

$$\mathrm{d}\xi/\mathrm{d}\tau = [1/2\mu(\mu+1)]\{\mu\xi + [\mu^2\xi^2 - 4\mu(1+\mu)]^{\frac{1}{2}}\}, \quad \xi(0) = c_0 \tag{40}$$

(this is essentially equation (26*c*) with a sign change). Equation (40) can be solved directly, to yield a solution similar to that given by equation (28*a*). However, the important difference here is that ξ now grows with τ, with

$$\xi \sim \mathrm{e}^{\tau/(\mu+1)}/2\mu, \quad y \sim \mathrm{e}^{\tau/(\mu+1)}/2(\mu+1), \quad x \sim 2(\mu+1)\,\mathrm{e}^{-\tau/(\mu+1)} \tag{41}$$

as $\tau \to \infty$. It is straightforward to show that this is a solution of the original system (19), to leading order, and no further time regions are required in this case. Equation (41) shows that ξ and y become unbounded and x decreases to zero on an $O(\epsilon^{-1})$ timescale. This form of behaviour can be seen in figure 7*b* for $\mu = 0.8$, $c_0 = 6.0$ and

$\epsilon = 0.01$ (the same parameter values, except for the sign change in ϵ as used in figure 6*b*). This shows that x and y evolve rapidly to the values given by equation (27*a*, *b*), while on a much longer timescale y increases and x decreases to zero.

The discussion of the case in which the initial behaviour is a damped oscillatory approach towards the 'non-zero' state (10*a*) also follows that given in the previous section. Now, the equation satisfied by $A_0(\tau)$ is

$$\mathrm{d}A_0/\mathrm{d}\tau = A_0, \tag{42a}$$

with solution

$$A_0 = c_0 \mathrm{e}^{\tau}, \tag{42b}$$

and with x_0 and y_0 given by equation (37) for τ sufficiently large. Thus in this case

$$x \sim [(\mu+1)/c_0\mu]\,\mathrm{e}^{-\tau}, \quad y \sim [c_0\mu/(\mu+1)]\,\mathrm{e}^{\tau} \tag{42c}$$

for τ large. This behaviour can be seen in figure 7*c*. There, an initial period of damped oscillation is followed by a slow decay of x and a slow increase in y (on an $O(\epsilon^{-1})$ timescale).

This completes the discussion of the case when $|\mu-\gamma| \ll 1$. We now go on to consider the general case when $|\mu-\gamma|$ is not necessarily small, in both the contracting and expanding scenarios. We start by examining the solution when c_0, the initial input of the autocatalyst B, is large.

6. The general case

The behaviour of any given system, with an arbitrary choice of parameter values, can be determined numerically, but even with μ and γ not of similar magnitude some analytical progress can be made, provided the initial autocatalyst concentration c_0 is large. Here, we examine two cases, namely (*a*) μ, γ of $O(1)$ and (*b*) μ, γ both of $O(c_0^{-1})$. The latter case is suggested by the earlier result for the reduced case that with $c_0 \gg 1$, the Hopf bifurcation arising for $\mu \sim c_0^{-1}$.

(*a*) *General case with* μ, γ *of* $O(1)$

With the parameters μ and γ of order unity, there is an initial region with duration of $O(1)$ in which

$$x = c_0^{-1}\bar{x}, \quad y = c_0\bar{y}, \quad \xi = c_0\bar{\xi}, \tag{43}$$

where $\bar{x}$, $\bar{y}$ and $\bar{\xi}$ are of $O(1)$. Substituting these scalings into equations (19), with t unscaled, gives

$$\mu(\bar{\xi}-\bar{y}) - \bar{x}\bar{y}^2 = c_0^{-2}(\mathrm{d}\bar{x}/\mathrm{d}t + \mu\bar{x}), \tag{44a}$$

$$\bar{x}\bar{y}^2 - \bar{y} = \mathrm{d}\bar{y}/\mathrm{d}t, \tag{44b}$$

$$\epsilon(\bar{\xi}-\bar{y}) - \mathrm{d}\bar{\xi}/\mathrm{d}t = c_0^{-2}\epsilon\bar{x}, \tag{44c}$$

with initial conditions (20) becoming

$$\bar{x}(0) = 0, \quad \bar{y}(0) = 1, \quad \bar{\xi}(0) = 1, \tag{44d}$$

where, as before, $\epsilon = \mu-\gamma$, but is now not necessarily small.

Equations (44) suggest an expansion of the form

$$\bar{x} = \bar{x}_0 + c_0^{-2}\bar{x}_1 + \ldots, \quad \bar{y} = \bar{y}_0 + c_0^{-2}\bar{y}_1 + \ldots, \quad \bar{\xi} = \bar{\xi}_0 + c_0^{-2}\bar{\xi}_1 + \ldots. \tag{45}$$

At leading order

$$\bar{x}_0\bar{y}_0^2 = \mu(\bar{\xi}_0 - \bar{y}_0) \tag{46a}$$

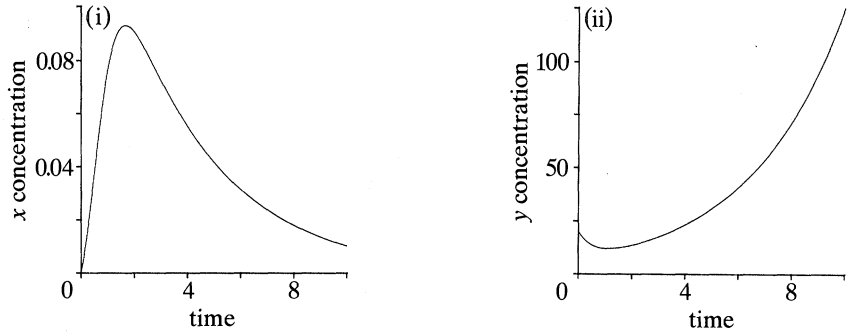

Figure 8. The behaviour for the general expanding case: $\mu = 1$, $\gamma = 0.5$ ($\epsilon = 0.5$), $c_0 = 20$.

and using this in equation (44*b*), we obtain

$$\mathrm{d}\bar{y}_0/\mathrm{d}t = \mu\bar{\xi}_0 - (\mu+1)\,\bar{y}_0, \tag{46b}$$

$$\mathrm{d}\bar{\xi}_0/\mathrm{d}t = \epsilon\bar{\xi}_0 - \epsilon\bar{y}_0. \tag{46c}$$

(i) *Expanding case*, $\epsilon > 0$

First we consider the expanding case, for which $\epsilon > 0$. The solution of equation (46) satisfying the initial conditions (44*d*) is

$$\bar{\xi}_0 = (\lambda_2 \mathrm{e}^{\lambda_1 t} - \lambda_1 \mathrm{e}^{\lambda_2 t})/(\lambda_2 - \lambda_1), \tag{47a}$$

$$\bar{y}_0 = [\lambda_2(\epsilon-\lambda_1)\,\mathrm{e}^{\lambda_1 t} - \lambda_1(\epsilon-\lambda_2)\,\mathrm{e}^{\lambda_2 t}]/\epsilon(\lambda_2-\lambda_1), \tag{47b}$$

$$\bar{x}_0 = \mu\epsilon^2(\lambda_2-\lambda_1)\,(\mathrm{e}^{\lambda_2 t} - \mathrm{e}^{\lambda_1 t})/[\lambda_2(\epsilon-\lambda_1)\,\mathrm{e}^{\lambda_1 t} - \lambda_1(\epsilon-\lambda_2)\,\mathrm{e}^{\lambda_2 t}]^2, \tag{47c}$$

where

$$\lambda_{1,2} = \tfrac{1}{2}\{\epsilon - (\mu+1) \mp [(\mu+1-\epsilon)^2 + 4\epsilon]^{\frac{1}{2}}\},$$

with $\epsilon > \lambda_2 > 0 > \lambda_1$.

A consideration of the higher order terms in equation (45) suggests that the expansion remains uniform with the asymptotic behaviour given by equation (47). From this we note that ξ and y both remain of $O(c_0)$ throughout and both become large for t large, with

$$\xi \sim \frac{c_0\,\epsilon\,\mathrm{e}^{\lambda_2 t}}{[(\mu+1-\epsilon)^2+4\epsilon]^{\frac{1}{2}}}, \quad y \sim \frac{c_0(-\lambda_1)\,(\epsilon-\lambda_2)\,\mathrm{e}^{\lambda_2 t}}{\epsilon[(\mu+1-\epsilon)^2+4\epsilon]^{\frac{1}{2}}} \tag{48a}$$

as $t \to \infty$. There is a difference between these two forms in that ξ increases monotonically, whereas y has a minimum at $t = (\lambda_2-\lambda_1)^{-1}\ln[(\epsilon-\lambda_1)/(\epsilon-\lambda_2)]$ before finally increasing. From equation (47*c*), x remains small – of $O(c_0^{-1})$ – throughout, approaching zero as

$$x \sim \frac{\mu\epsilon^2[(\mu+1-\epsilon)^2+4\epsilon]^{\frac{1}{2}}}{\lambda_1^2(\epsilon-\lambda_2)^2}\,\mathrm{e}^{-\lambda_2 t} \tag{48b}$$

as $t \to \infty$. Note that these forms agree with equation (41) when $\epsilon \ll 1$.

The behaviour described above can be seen in figure 8, for a system with $\mu = 1$, $\gamma = 0.5$ (so $\epsilon = 0.5$) and $c_0 = 20$. The minimum in y is seen, with the large time behaviour of both x and y as given by equation (48*a*, *b*).

(ii) *Contracting case*, $\epsilon < 0$

Next, we consider the contracting case, with $\epsilon < 0$. For this, we take $\delta = \gamma - \mu > 0$, with now δ not necessarily small. The solution for the leading order term is still given by equation (47), with ϵ replaced by $-\delta$, though now $\lambda_1 < \lambda_2 < 0$. The behaviour as

$t \to \infty$ is given by equation (48), but now we should expect that $\xi_0 \to 0$, $y_0 \to 0$ and $x_0 \to \infty$. Thus, expansion (45) becomes non-uniform and to determine the timescale over which this develops, we need to consider terms of $O(c_0^{-2})$ in expansion (45). This gives for $\bar{y}_1$ and $\bar{\xi}_1$, on using equation (44*a*)

$$\mathrm{d}\bar{y}_1/\mathrm{d}t = \mu\bar{\xi}_1 - (\mu+1)\,\bar{y}_1 - \mathrm{d}\bar{x}_0/\mathrm{d}t - \mu\bar{x}_0, \tag{49a}$$

$$\mathrm{d}\bar{\xi}_1/\mathrm{d}t = \delta(\bar{y}_1 - \bar{\xi}_1 + \bar{x}_0). \tag{49b}$$

Equations (49) possess a complementary function of the form given by equation (47), which will die away as $t \to \infty$, and a particular integral (via the term in x_0) which has

$$\xi_1 \sim \frac{\mu\delta^3(\lambda_2-\lambda_1)\,(\mu\lambda_2+\mu-\lambda_2)\,\mathrm{e}^{-\lambda_2 t}}{\lambda_1^2(\delta+\lambda_2)^2(\delta-\lambda_2\,\delta-\mu\lambda_2-\lambda_2+\lambda_2^2)} \tag{49c}$$

as $t \to \infty$. This shows that expansion (45) becomes non-uniform when t is of $O(-\lambda_2^{-1}\ln(c_0))$ with then x, y and ξ all of $O(1)$.

To continue, we put $t = -\lambda_2^{-1}\ln(c_0) + \bar{t}$ and leave x, y and ξ unscaled. This leaves equation (19) unaltered (except that t is replaced by $\bar{t}$) with

$$\left.\begin{aligned} x &\sim \frac{\mu\delta^2(\lambda_2-\lambda_1)}{\lambda_1^2(\lambda_2+\delta)}\mathrm{e}^{-\lambda_2\bar{t}} + O(\mathrm{e}^{-3\lambda_2\bar{t}}),\\ y &\sim \frac{-\lambda_1(\lambda_2+\delta)}{\delta(\lambda_2-\lambda_1)}\mathrm{e}^{\lambda_2\bar{t}} + O(\mathrm{e}^{-\lambda_2\bar{t}}),\\ \xi &\sim \frac{-\lambda_1}{(\lambda_2-\lambda_1)}\mathrm{e}^{\lambda 2\bar{t}} + O(\mathrm{e}^{-\lambda 2\bar{t}}) \end{aligned}\right\} \tag{50}$$

as $\bar{t} \to \infty$ (note that $\lambda_2 < 0$).

A consideration of equation (19) with $\delta = -\epsilon > 0$ shows that $y \to 0$ whilst x and ξ approach the same constant value as $\bar{t} \to \infty$. This final value is not determinable from the above analysis and requires a solution of the full problem.

This behaviour can be seen from the results shown in figure 9, taking $\mu = 1$, $\gamma = 1.5$ (so $\delta = 0.5$) and $c_0 = 20$. This shows that y tends to zero monotonically, while a double structure in the behaviour of x is seen, with x finally approaching a non-zero constant value.

(*b*) *General case with* μ, γ *of* $O(c_0^{-1})$

Next, we consider the case when μ and γ are both of $O(c_0^{-1})$ for $c_0 \gg 1$. Here we put $\mu = \bar{\mu}c_0^{-1}$, $\epsilon = \bar{\epsilon}c_0^{-1}$ (or $\delta = \bar{\delta}c_0^{-1}$) where $\bar{\mu}, \bar{\epsilon}$ (or $\bar{\delta}$) are of $O(1)$. An initial region is now required in which

$$x = c_0^{-2}X, \quad y = c_0\,Y, \quad \xi = c_0\,\zeta \tag{51}$$

and t is left unscaled. Equations (19) become

$$c_0^{-2}\,\mathrm{d}X/\mathrm{d}t = \bar{\mu}(\zeta - Y) - XY^2 - c_0^{-3}\,\bar{\mu}X, \tag{52a}$$

$$\mathrm{d}Y/\mathrm{d}t = -Y + c_0^{-1}XY^2, \tag{52b}$$

$$\mathrm{d}\zeta/\mathrm{d}t = c_0^{-1}\,\bar{\epsilon}(\zeta - Y) - c_0^{-4}\,\bar{\epsilon}X \tag{52c}$$

subject to initial conditions

$$X(0) = 0, \quad Y(0) = 1, \quad \zeta(0) = 1. \tag{52d}$$

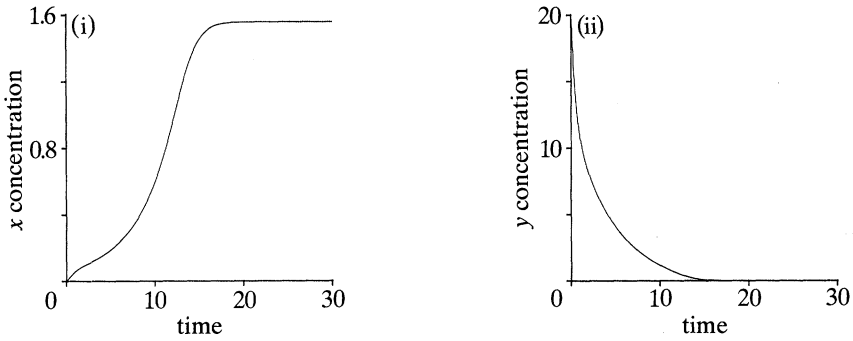

Figure 9. The behaviour for the general contracting case: $\mu = 1$, $\gamma = 1.5$ ($\delta = 0.5$), $c_0 = 20$.

An expansion in powers of c_0^{-1} is suggested by equation (52) with, at leading order,

$$X_0 = \bar{\mu}\,\mathrm{e}^{2t}(1-\mathrm{e}^{-t}), \quad Y_0 = \mathrm{e}^{-t}, \quad \zeta_0 = 1. \tag{53a}$$

This shows that X_0 grows with t and a consideration of the terms of $O(c_0^{-1})$ is required. These give

$$\left.\begin{aligned} X_1 &= \mathrm{e}^{2t}\{\bar{\mu}\bar{\epsilon}(t-\mathrm{e}^{-t}-1)-\bar{\mu}^2[1+2\mathrm{e}^{t}(1-\mathrm{e}^{-t})]\,(1-t\,\mathrm{e}^{-t}-\mathrm{e}^{-t})\},\\ Y_1 &= \bar{\mu}(1-t\,\mathrm{e}^{-t}-\mathrm{e}^{-t}), \quad \zeta_1 = \bar{\epsilon}(t+\mathrm{e}^{-t}-1). \end{aligned}\right\} \tag{53b}$$

Thus the expansion breaks down when t is of $O(\ln c_0)$ with then x and y both of $O(1)$. This suggests putting

$$t = \ln(c_0) + \bar{t}, \quad \xi = c_0\,\bar{\xi} \tag{54}$$

and leaving x and y unscaled. Substituting these forms into equation (19), an expansion in inverse powers of c_0 is suggested. This in turn leads to $\bar{\zeta} = 1 + \bar{\epsilon}\bar{t}c_0^{-1} + \ldots$, which becomes non-uniform on an $O(c_0)$ timescale. To discuss the solution further in this region, we use a two-timescale analysis, with $\bar{t}$ and $\tau = c_0^{-1}\bar{t}$ as the fast and slow time variables respectively, and looking for a solution by expanding in inverse powers of c_0.

The equation for $\bar{\zeta}_0$, the leading term in the expansion for $\bar{\zeta}$, is

$$\partial\bar{\zeta}_0/\partial t = 0, \quad \bar{\zeta}_0 \to 1 \quad \text{as} \quad \bar{t} \to -\infty, \tag{55a}$$

giving

$$\bar{\zeta}_0 = B_0(\tau), \quad B_0(0) = 1, \tag{55b}$$

for some, as yet undetermined, function $B_0(\tau)$. The equations for x_0 and y_0 (the leading terms in the expansions for x and y respectively) are then

$$\mathrm{d}x_0/\mathrm{d}t = \bar{\mu}B_0(\tau) - x_0\,y_0^2, \tag{55c}$$

$$\mathrm{d}y_0/\mathrm{d}t = x_0\,y_0^2 - y_0 \tag{55d}$$

subject to, from equation (53),

$$x_0 \sim \bar{\mu}\,\mathrm{e}^{2\bar{t}} - 2\bar{\mu}^2\,\mathrm{e}^{3\bar{t}} + \ldots, \quad y_0 \sim \bar{\mu} + \ldots \quad \text{as} \quad \bar{t} \to \infty.$$

At $O(c_0^{-1})$, we have, using equation (55*b*),

$$\mathrm{d}\bar{\zeta}_1/\mathrm{d}t = \bar{\epsilon}B_0 - \mathrm{d}B_0/\mathrm{d}\tau, \quad \bar{\zeta}_1(0) = 0. \tag{56a}$$

To remove the secular terms arising at this stage and to render the expansion uniform for times of $O(c_0)$, we must have, from equation (56*a*)

$$B_0(\tau) = \mathrm{e}^{\bar{\epsilon}\tau} \tag{56b}$$

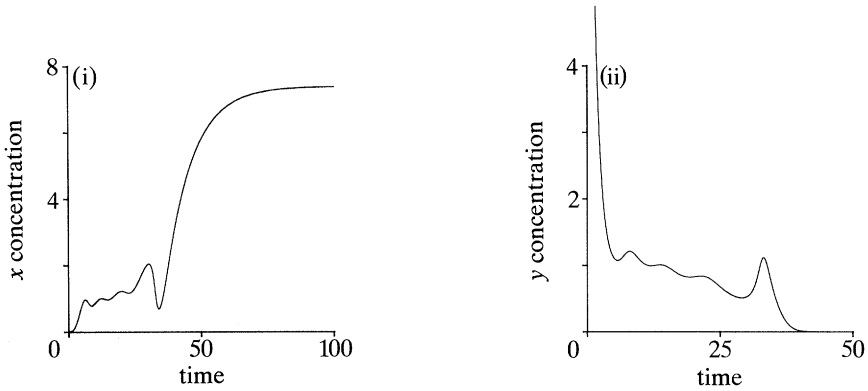

Figure 10. The behaviour for the general contracting case with μ and γ of $O(c_0^{-1})$: $\mu = 0.075$, $\gamma = 0.1$, $c_0 = 20$.

With this form for $B_0(\tau)$ and $\epsilon < 0$, equation (55c, d) become the same as those considered in some detail by Merkin *et al.* (1986). Hence, for the contracting case starting (say) with a value of $\bar{\mu} > 1$, it follows from that earlier study that there is a region where the solution follows the quasi-steady state

$$x_0 = \bar{\mu}^{-1} \mathrm{e}^{\bar{\delta}\tau}, \quad y_0 = \bar{\mu}\, \mathrm{e}^{-\bar{\delta}\tau} \qquad (\text{where } \bar{\delta} = -\bar{\epsilon} > 0). \tag{57}$$

this is followed by the onset of a region of oscillatory behaviour of increasing amplitude and period, arising from the equivalent of a Hopf bifurcation at $\tau = \bar{\delta}^{-1} \ln(\bar{\delta})$. This period of oscillatory behaviour ends, through the infinite period bifurcation at time $t_c = (c_0/\bar{\delta}) \ln(\bar{\mu}/\bar{\mu}_c)$ where, as before, $\bar{\mu}_c = 0.90032$. After this, $y \to 0$ exponentially quickly and, with $t_1 = \bar{t} - t_c$, $x \sim \bar{\mu}_c t_1$ and $\xi \sim c_0 \bar{\mu}_c/\bar{\mu}$ on a t_1 of $O(1)$ timescale. To complete the solution we put $y \equiv 0$ and

$$x = c_0 X, \quad \xi = c_0 F, \quad \tau_1 = c_0^{-1} t_1, \tag{58a}$$

with equations (19) then reducing to

$$\mathrm{d}X/\mathrm{d}\tau_1 = \bar{\mu}(F - X), \quad \mathrm{d}F/\mathrm{d}\tau_1 = -\bar{\delta}(F - X), \tag{58b}$$

$$X \sim \mu_c \tau_1, \quad F \sim \bar{\mu}_c/\bar{\mu} \quad \text{for} \quad \tau_1 \ll 1. \tag{58c}$$

Equation (58a–c) have the solution

$$X = [\bar{\mu}_c/(\bar{\mu} + \bar{\delta})][1 - \exp(-(\bar{\mu} + \bar{\delta})\tau_1)], \quad F = [\bar{\mu}_c/(\bar{\mu} + \bar{\delta})][1 + \bar{\delta}/\bar{\mu} \exp(-(\bar{\mu} + \bar{\delta})\tau_1)]. \tag{60a}$$

From (60a) it follows that finally x and ξ tend to the same limit, namely

$$x, \xi \to \bar{\mu}_c c_0/(\bar{\mu} + \bar{\delta}). \tag{60b}$$

This behaviour is illustrated in figure 10 for the system with $\mu = 0.075$ ($\bar{\mu} = 1.5$), $c_0 = 20$ and $\epsilon = -0.025$ ($\bar{\delta} = 0.5$).

For the expanding case, $\bar{\epsilon} > 0$, the solution of equation (55c, d) becomes stable as τ increases, with ultimately

$$x \sim \bar{\mu}^{-1} \mathrm{e}^{-\bar{\epsilon}\tau}, \quad y \sim \bar{\mu}\, \mathrm{e}^{\bar{\epsilon}\tau} \quad \text{as} \quad \tau \to \infty. \tag{61}$$

If we start with $\mu < 1$, a region of oscillatory behaviour will be seen before the final quasi-steady state evolution is attained. This behaviour is seen in the results shown in figure 11, taking $\mu = 0.0475$ ($\bar{\mu} = 0.95$), $c_0 = 20$ and $\epsilon = 0.025$. There is an initial

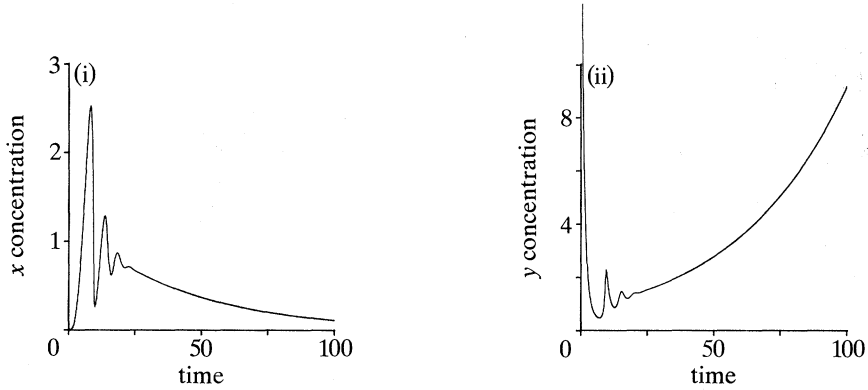

Figure 11. The behaviour for the general expanding case with μ and γ of $O(c_0^{-1})$: $\mu = 0.0475$, $\gamma = 0.0225$, $c_0 = 20$.

period of oscillatory behaviour (since μ starts in the interval $\bar{\mu}_c < \bar{\mu} < 1$) which is followed, after a time of $O(\epsilon^{-1} \ln \bar{\mu})$ by monotonic evolution following the above asymptotic forms.

7. Discussion

In the previous sections we have examined in some detail the evolution of a model based on the product-feedback autocatalator scheme of Peng *et al.* (1989). The main difference between the original and the form used here is that two 'uncatalysed' reactions (the direct production of A from P and the direct conversion of A and B) that compete with the catalysed steps (1*a*) and (1*b*) have been omitted. There are some significant consequences of this reduction. Now, only in the special case that $\mu = \gamma$, or in dimensional terms $k_0 p_0 = k_3$, does the system have a recognizable structure of non-trivial stationary state and limit cycle behaviour (under the usual 'pool chemical approximation'). The equality of the two pseudo-first-order rate coefficients means that a molecule C is equally likely to participate in the initiation process (1*a*), and thus provide more active intermediate species, or to decay to the stable product D via the 'termination' process (1*d*). Under these somewhat restrictive conditions, the system then provides a classic example of multistability and Hopf bifurcation phenomena, with extinction of oscillations occurring through homoclinic orbit bifurcations arising from a double zero eigenvalue degeneracy. The Hopf bifurcation shows a second degeneracy, with the stability of the merging limit cycle changing from unstable to stable at an $H3_1$ point (Gray & Roberts 1988).

For the more general case, in which $k_0 p_0$ and k_3 are not exactly equal, this stationary state structure collapses. For the 'contracting' case, with $k_0 p_0 < k_3$ the termination process wins out, on average, so the concentrations of the two catalytic intermediates B and C decrease in time, tending to a final state with [B] = [C] = 0 (but a non-zero, steady final concentration of intermediate A). For the 'expanding' case, with $k_0 p_0 > k_3$, a molecule of C is more likely to react via the initiation channel than in the termination step. The future course is then determined by the competition between steps (1*b*) and (1*c*). The overall reaction may still 'die out', with [B] and [C] tending to zero and [A] tending to a non-zero constant given by the initial concentration of the intermediates. However, for other parameter values, a growing solution can be attained, with [B] and [C] becoming unbounded (in the 'pool chemical approximation') and [A] tending (slowly) to zero.

Despite the rather special nature of the 'reduced' case, with μ exactly equal to γ, the understanding developed there in §3 proved to be extremely valuable in providing a framework for both general cases. The evolving concentrations could clearly be seen to follow the same stationary state and limit cycle structure quasi-steadily. The analysis based on this information allowed the final intermediate concentrations to be determined asymptotically.

The unbounded growth for the 'expanding' case is the most severely modified part of the behaviour when the pool chemical approximation is relaxed (i.e. when the consumption of the precursor species P is admitted). This decay is governed by the equation

$$\mathrm{d}[\mathrm{P}]/\mathrm{d}t' = -k_0 pc.$$

In the dimensionless terms used above, this can be rewritten as

$$\mathrm{d}\mu/\mathrm{d}t = -\eta\mu z,$$

where $\eta = k_0/(k_1 k_2)^{\frac{1}{2}}$. For the pool chemical approximation to apply, we require $\eta \ll 1$, so the right hand side of this equation remains small for a sufficiently long period. In such cases, the decay of P simply adds a slow decrease in the effective value for μ to the decay in c_0 described earlier, and enhances slightly the departure from the (quasi-steady) stationary state (10a) or the stable limit cycle surrounding it. In the 'expanding' case, the unbounded growth will be curtailed and the system tends back to $[\mathrm{B}] = [\mathrm{C}] = 0$ at the very longest times.

Strictly, the model studied here is structurally unstable to the re-introduction of the two steps discussed above. The particular choice of the model has been guided by longer term interests connected with chemical wave propagation, as described earlier. It is, however, interesting to consider the differences between the present scheme and its 'full' form (Peng *et al.* 1990; Scott *et al.* 1991). The latter, crucially contains the step $\mathrm{P} \rightarrow \mathrm{A}$, with rate $= k_p p_0$ (say). The system then exhibited Hopf bifurcation, period doubling and chaos. In terms of the dimensionless equations this is equivalent to modifying equation (4a) to

$$\mathrm{d}x/\mathrm{d}t = \nu + \mu z - xy^2, \tag{62}$$

where $\nu = (k_p k_1^{\frac{1}{2}} p_0/k_2^{\frac{3}{2}})$ with equation (4b, c) unaltered. The system given by (4b, c) and (62) has the single stationary state

$$x_{\mathrm{ss}} = (\gamma-\mu)/\gamma\nu, \quad y_{\mathrm{ss}} = \gamma\nu/(\gamma-\mu), \quad z_{\mathrm{ss}} = \nu/(\gamma-\mu), \tag{63}$$

provided $\gamma > \mu$; for the 'expanding case', $\gamma \leqslant \mu$, the system has no finite stationary state.

The unique stationary state (63) can lose local stability (for acceptable parameter values) at points of Hopf bifurcation given by

$$\gamma^3(\gamma+1)\nu^4 - \gamma(1+2\gamma-\gamma^2-\mu)(\gamma-\mu)^2\nu^2 - (\gamma-1)(\gamma-\mu)^4 = 0, \tag{64}$$

with $\gamma > \mu$. Note that equation (64) reduces to $\nu = 1$ when $\mu = 0$ (Merkin *et al.* 1987b). The emerging limit cycle from this primary bifurcation may then undergo secondary bifurcations, giving the complex dynamical behaviour reported by Peng *et al.* (1990). In our case, however, the only stationary state for $\gamma > \mu$ is $y_{\mathrm{ss}} = z_{\mathrm{ss}} = 0$ with x_{ss} being some positive constant and this state is a stable node for all parameter values (although some transient oscillatory development is possible). In the special case $\gamma = \mu$, other stationary state solutions and Hopf bifurcations are possible, but

this has reduced the model to two independent variables, so again secondary bifurcations and the ensuing more complex responses are not allowed. We are grateful to a referee for showing that bounded chaotic behaviour is not possible in this system, the proof of which is given in the Appendix.

Finally, it is interesting to recognize that the original autocatalator scheme also emerges naturally from our model, in the limit of large c_0; both for the reduced scheme and, perhaps more significantly, for the general case when $|\mu-\gamma|$ is not small (see §6). A large value of c_0 corresponds to a large initial input of the autocatalyst B, with the concentrations of A and C remaining small, at least initially. With the concentration of C low, the final termination step ($1d$) is relatively weak and the scheme reduces to that discussed previously (Merkin *et al.* 1986, 1987*a*, *b*) with the difference that the initiation step is now catalysed by the 'product' C. With low initial concentrations of C, this latter point effectively provides a slowly varying value for the parameter μ, evolving quasi-statically with the solution.

We are grateful to an anonymous referee for the proof in the Appendix, and to SERC (SMC) and NATO (SKS, grant no. 0124/89) for financial support.

Appendix

Result. *The solution of the initial-value problem consisting of equation* ($4a$–c) *subject to* $x(0) = 0$, $y(0) = c_0 > 0$ $z(0) = 0$ *cannot approach a bounded chaotic attractor as* $t \to \infty$, *for any* $\mu, \gamma > 0$.

Proof. Let $x = x_e(t)$, $y = y_e(t)$, $z = z_e(t)$ be the solution to the initial-value problem in $t > 0$. The quadrant $x, y, z \geqslant 0$ is readily shown to be invariant for equation ($4a$–c), and so, $x_e(t)$, $y_e(t)$, $z_e(t) \geqslant 0$ for all $t > 0$. Hence

$$\mathrm{d}(x_e(t)+y_e(t)+z_e(t))/\mathrm{d}t = (\mu-\gamma)\, z_e(t) \begin{cases} \geqslant 0, & \mu > \gamma, \\ \leqslant 0, & \mu < \gamma \end{cases}$$

for all $t > 0$. Thus $\mu > \gamma (\mu < \gamma)$ $x_e(t)+y_e(t)+z_e(t)$ is monotone increasing (decreasing) with t. Now suppose that the solution approaches a bounded chaotic attractor as $t \to \infty$. Then certainly all of $x_e(t)$, $y_e(t)$, $z_e(t)$ are bounded above and below as $t \to \infty$, and it follows that so is $(x_e(t)+y_e(t)+z_e(t))$. Therefore, for $\mu > \gamma (\mu < \gamma)$ $(x_e(t)+y_e(t)+z_e(t))$ is monotone increasing (decreasing) and bounded above (below), and so there is a positive constant c_∞ such that (in both cases), $(x_e(t)+y_e(t)+z_e(t)) \to c_\infty$ as $t \to \infty$. Hence the asymptotic dynamics of the initial-value problem as $t \to \infty$ takes place on the two-dimensional manifold $x+y+z = c_\infty$, and are therefore governed by the autonomous two dimensional system,

$$\mathrm{d}x/\mathrm{d}t = \mu[c_\infty - x - y] - xy^2, \quad \mathrm{d}y/\mathrm{d}t = xy^2 - y,$$

which leads to a contradiction as this system cannot have a chaotic attractor. The result follows. □

References

Billingham, H. & Needham, D. J. 1991*a* The development of travelling waves in quadratic and cubic autocatalysis with unequal diffusion rates. I. Permanent form travelling waves. *Phil. Trans. R. Soc. Lond.* A **334**, 1–24.

Billingham, J. & Needham, D. J. 1991*b* The development of travelling waves in quadratic and cubic autocatalysis with unequal diffusion rates. II. An initial-value problem with an immobilized or nearly immobilized autocatalyst. *Phil. Trans. R. Soc. Lond.* A **336**, 497–539.

Forbes, L. A. 1990 Limit cycle behaviour in a model chemical reaction: the Sal'nikov thermokinetic oscillator. *Proc. R. Soc. Lond.* A **430**, 641–651.

Forbes, L. A. & Holmes, C. A. 1990 Limit cycle behaviour in a model chemical reaction: the cubic autocatalator. *J. Engng Math.* **24**, 179–189.

Gray, B. F. & Roberts, M. J. 1988 A method for the complete qualitative analysis of two coupled ordinary differential equations dependent on three parameters. *Proc. R. Soc. Lond.* A **416**, 361–389.

Gray, B. F., Roberts, M. J. & Merkin, J. H. 1988 The cubic autocatalator: the influence of quadratic autocatalytic and uncatalysed reactions. *J. Engng Math.* **22**, 267–284.

Gray, B. F., Roberts, M. J. & Merkin, J. H. 1989 On the structural stability of the cubic autocatalytic scheme in a closed vessel. *Dynam. Stabil. Syst.* **4**, 31–54.

Gray, P. 1988 Instabilities and oscillations in chemical reactions in closed and open systems. *Proc. R. Soc. Lond.* A **415**, 1–34.

Gray, P. & Scott, S. K. 1986 A new model for oscillatory behaviour in closed systems: the autocatalator. *Ber. BunsenGes. phys. Chem.* **90**, 985–996.

Hassard, B. D., Kazarinoff, N. D. & Wan, Y.-H. 1980 *Theory and applications of the Hopf bifurcation*. Cambridge University Press.

Kaas-Petersen, C. & Scott, S. K. 1988 Homoclinic orbits in a simple model of an autocatalytic reaction. *Physica* D **32**, 461–470.

Merkin, J. H. & Needham, D. J. 1990 Reaction-diffusion in a simple pooled chemical system. *Dynam. Stabil. Syst.* **4**, 141–167.

Merkin, J. H., Needham, D. J. & Scott, S. K. 1986 Oscillatory chemical reactions in closed vessels. *Proc. R. Soc. Lond.* A **406**, 299–323.

Merkin, J. H., Needham, D. J. & Scott, S. K. 1987*a* On the structural stability of a simple pooled chemical system. *J. Engng Math.* **21**, 115–127.

Merkin, J. H., Needham, D. J. & Scott, S. K. 1987*b* On the creation, growth and extinction of oscillatory solutions for a simple pooled chemical reaction scheme. *SIAM J. appl. Math.* **47**, 1040–1060.

Peng, B., Scott, S. K. & Showalter, K. 1990 Period-doubling and chaos in a three variable autocatalator. *J. phys. Chem.* **94**, 5243–5246.

Scott, S. K. & Tomlin, A. S. 1990 Period-doubling and chaotic sequences in the simplest chemical systems. *Phil. Trans. R. Soc. Lond.* A **332**, 51–68.

Scott, S. K., Peng, B., Tomlin, A. S. & Showalter, K. 1991 Transient chaos in a closed chemical system. *J. chem. Phys.* **94**, 1134–1140.

Verhulst, F. 1990 *Nonlinear differential equations and dynamical systems*. Springer-Verlag.

Received 26 April 1991; revised 13 November 1991; accepted 18 February 1992

PHILOSOPHICAL TRANSACTIONS OF THE ROYAL SOCIETY A MATHEMATICAL, PHYSICAL & ENGINEERING SCIENCES